Radiation trapping under conditions of low to moderate line-center optical depth

T. Colbert and J. Huennekens
Department of Physics, Lehigh University, Bethlehem, Pennsylvania 18015
(Received 27 December 1989)

We have studied trapping of resonance radiation under conditions of moderate to low line-center optical depths in sodium-argon mixtures. We report measured effective radiative decay rates, which are compared with predictions of the Post [Phys. Rev. A **33**, 2003 (1986)] and the Milne [J. Lond. Math. Soc. **1**, 40 (1926)] theories of radiation trapping. These theories are expected to be valid for spectral lines with low to moderate line-center optical depths, where the commonly used Holstein [Phys. Rev. **72**, 1212 (1947); **83**, 1159 (1951)] theory of radiation trapping is expected to break down. The experiment was performed under conditions in which the trapping was dominated by either the Doppler-broadened Gaussian or by the impact-broadened Lorentzian line-shape function. The measured effective radiative decay rates agree well with those predicted by the Milne and Post theories over the range of low to moderate optical depth.

I. INTRODUCTION

Radiation trapping refers to a decrease in the effective radiative decay rate of a resonance line due to repeated absorption and reemission of photons. In an atomic vapor, such as sodium, resonance radiation may undergo many such reabsorptions before escaping from the region containing the vapor. The average number of reabsorptions taking place determines the effective radiative decay rate. This effective radiative rate is given by

$$\Gamma_{\text{eff}}=g\Gamma_{\text{nat}}\ , \tag{1}$$

where the escape factor g is the inverse of the mean number of absorption events, and Γ_{nat} is the natural radiative rate.[1,2] The escape factor depends on the spectral line shape, the absorbing atom density, and the geometry of the region from which light is escaping. An understanding of the trapping process is important in order to correctly model energy transport in optically thick plasmas and neutral atom vapors. Such considerations are particularly important in the accurate modeling of stellar atmospheres and discharge lamps.

In previous experiments, we have confirmed the validity of the Holstein theory of radiation trapping for a wide range of experimental conditions.[3,4] Under conditions of high optical depth, ideal geometry, complete frequency redistribution, and a single line-broadening mechanism, the Holstein theory predictions for the effective radiative decay rates agree well with measured decay rates. Radiative decay rates were measured for conditions where either Doppler broadening or impact broadening dominated the radiation trapping process (i.e., the unity optical depth points $k(\omega)l\sim 1$ occurred in the Doppler core or in the pressure-broadened wings, respectively[4]). The cell geometry was made to approximate an infinite slab.

In the present work, radiative decay rates are measured for conditions of low to moderate optical depths, where the Holstein theory is expected to break down. Effective decay rates (Γ_{eff}) or escape factors (g) are compared with values predicted from the Holstein,[1,2] Milne,[5] and Post,[6] theories of radiation trapping. Decay rates are measured for conditions where the trapping is dominated by either Doppler or impact broadening. Comparison of measured decay rates with the theoretical values yields the range of optical depths for which each of these theories is valid.

II. REVIEW OF THEORY

In order to predict escape factors, knowledge is required of the spatial distribution of absorbing atoms, the excitation geometry, the frequency-dependent absorption coefficient $k(\omega)$, the frequency and angular redistribution functions, and the relevant collisional excitation transfer rates. Given such information, one can accurately determine escape factors using Monte Carlo computer simulations.[7] However, these calculations are expensive, and it is not obvious how the numerical results scale when one, for example, changes the species of absorbing atoms or the cell dimension.

Many theories have been developed which predict escape factors using various simplifying approximations.[1,2,5,6,8,9] Holstein[1,2] derived simple closed-form expressions for the escape factor for conditions of high line-center optical depth [$k(\omega_0)l\gg 1$, where $k(\omega_0)$ is the line-center absorption coefficient and l is a geometric factor], a single line-broadening mechanism, complete frequency redistribution (i.e., no correlation between emitted and absorbed photon frequencies), and an ideal geometry. It has been shown that the Holstein theory yields accurate values for the escape factor when experimental conditions satisfy the above assumptions.[3,4] In the present work, we study radiation trapping under conditions of low to moderate line-center optical depth. For such conditions, the simple Holstein theory expressions can give a nonphysical radiative rate which is faster than the natural radiative rate. However, our present results test the strictness of the high-optical-depth assumption.

The Holstein theory results for the escape factors are given here for the cases of Doppler broadening and

impact-regime pressure broadening, respectively (for an infinite slab of thickness L):

$$g=\begin{cases}1.875(k(\omega_0)L\{\pi\ln[k(\omega_0)L/2]\}^{1/2})^{-1} & \text{(Doppler)} \quad (2a)\\ 1.150[\pi k(\omega_0)L]^{-1/2} & \text{(impact)} . \quad (2b)\end{cases}$$

The absorption coefficient is, in general, given by

$$k(\omega)=\left[\frac{\lambda^2 g_2}{4g_1}\Gamma_{\text{nat}}n\right]F(\omega)=\kappa F(\omega) , \quad (3)$$

where κ is simply defined by Eq. (3), λ is the transition wavelength, g_2 and g_1 are upper- and lower-state statistical weights, respectively, n is the absorbing atom density, and $F(\omega)$ is the appropriate normalized line-shape function [$\int d\omega F(\omega)=1$].

In the Holstein theory (and each of the other theories discussed below), a more general solution to the radiation diffusion equation is an eigenmode expansion of the following form:

$$n_e(\mathbf{r},t)=\sum_i C_i n_i(\mathbf{r})\exp(-\beta_i t) . \quad (4)$$

Here $n_e(\mathbf{r},t)$ is the excited atom density at position $\mathbf{r}$ and time t, and the $n_i(\mathbf{r})$ form a complete set of spatial eigenmodes, each of which is a mathematical solution to the radiation diffusion equation corresponding to a pure exponential decay $e^{-\beta_i t}$. C_i is the amplitude and β_i is the decay rate of the ith mode. The fundamental mode $i=1$ is the slowest decaying mode ($\beta_1<\beta_i$, $i\neq 1$), and is the only one which must be considered in the present experiments. This point will be discussed further in Sec. IV A. In this paper all expressions for g obtained from the various theories yield escape factors for the fundamental spatial mode (i.e., $\beta_1\equiv\Gamma_{\text{eff}}=g\Gamma_{\text{nat}}$).

In addition to the Holstein theory, we also consider two theories which are expected to be valid for conditions where $\mathbf{k}(\omega_0)l\lesssim 5$; i.e., those due to Milne[5] and Post.[6,10] Both of these theories yield expressions for the escape factor which, in general, require numerical evaluation. In order to simplify these calculations, we perform the experiment under conditions where the trapping is well described by a single line-broadening mechanism; i.e., the line shape is well described by either the Doppler (Gaussian) or the impact-broadened Lorentzian function.

The starting point for the Milne theory is a radiation diffusion equation in which the spectral line is described by an equivalent opacity.[5] This is equivalent to assuming a mean free path for the absorption of photons in the vapor.[1] While it has been shown that a mean free path cannot in general be defined for this problem,[1] it should be a valid approximation at low optical depths. The equivalent opacity $\overline{kl}$ can be defined by[11–13]

$$\exp(-\overline{kl})=\int \mathbf{F}(\omega)\exp[-k(\omega)l]d\omega . \quad (5)$$

The geometric factor is not well defined in the literature, but we will use $l=L$ for the slab of thickness L since we have found that this definition yields the best agreement with experimental results. In this case, Milne's solution for the escape factor is

$$g=[1+(\overline{kL}/\epsilon)^2]^{-1} , \quad (6)$$

where ϵ is the first root of

$$\epsilon\tan(\epsilon)=\overline{kL} . \quad (7)$$

While these results are not as easy to use as the Holstein results, all the necessary computations can be performed fairly rapidly on a personal computer (assuming a simple line shape). Isotope shifts and hyperfine structure can also be accommodated in this model, in contrast to the high-optical-depth Holstein theory which can only incorporate such structure in an *ad hoc* manner.

The Post theory offers a more general solution to the radiation diffusion problem.[6,10] This theory can accommodate a realistic Voigt line shape, isotopic and hyperfine structure, and incomplete frequency redistribution. Additionally, it is expected to be valid over the entire range of line-center optical depths. The disadvantage of the Post theory is that it is much more difficult to use than the simple Holstein and Milne theory expressions.

The Post theory starts off with a diffusion equation similar to that used by Holstein, but which takes into account the possibility of incomplete frequency redistribution in a manner first introduced by Payne *et al.*[14] The issue of when incomplete frequency redistribution effects are important has been discussed repeatedly in the literature.[6,10,14–16] However, in one case where this effect was important,[10] the Post theory was shown to work well. The Post theory has also been used successfully to analyze experimental results in two cases where hyperfine structure was important.[10,15] In analyzing the present set of experiental results, we will make some approximations to the Post theory which are valid for our low to moderate optical-depth conditions.

Assuming complete frequency redistribution (which is valid for Doppler and pressure broadening[14]) and a single line-broadening mechanism (which is valid for our condition as we shall demonstrate in Secs. IV B and IV C), we obtain the following Post-theory expression for the escape factor:

$$g=\int_0^\infty d\omega\, F(\omega)\eta(\tau) . \quad (8)$$

Here $F(\omega)$ is the line-shape function, either Doppler or Lorentzian, $\tau=k(\omega)L/2$ is the Post-theory definition for the optical depth at frequency ω for a slab of thickness L, and the escape function $\eta(\tau)$ contains all of the spatial information of the problem.[6] $F(\omega)$ and $\eta(\tau)$ are defined as follows:[6]

$$F(\omega)=\begin{cases}\dfrac{2}{\Delta\omega_D}\left[\dfrac{\ln(2)}{\pi}\right]^{1/2}\exp\left[-4\ln(2)\left[\dfrac{\Delta\omega}{\Delta\omega_D}\right]^2\right] & \text{(Doppler)} , \quad (9a)\\ \dfrac{\Gamma_c/(2\pi)}{\Delta\omega^2+(\Gamma_c/2)^2} & \text{(Lorentzian)} , \quad (9b)\end{cases}$$

for Doppler and Lorentizan line shapes, and

$$\eta(\tau)\approx 1-\int_V d\rho\,\tau(\omega)\frac{\exp[-\tau(\omega)|\rho|]}{4\pi|\rho|^2}f(\rho)\ . \tag{10}$$

Here $\Delta\omega=\omega-\omega_0$ is the frequency referenced to the line-center frequency ω_0, Γ_c is the impact-broadened linewidth [full width at half maximum (FWHM) in angular frequency units], $\Delta\omega_D$ is the Doppler linewidth, and ρ is a dimensionless position coordinate ($\rho=2x/L$) which varies over the slab volume V. The origin is taken to be the slab center. $f(\rho)$ is the fundamental mode excited atom distribution normalized to one at the slab center [$f(\rho)\equiv n_1(\rho)/n_1(0)$]. The Post-theory escape function $\eta(\tau)$ cannot, in general, be expressed in closed form. However, to simplify calculations, we approximate $\eta(\tau)$ by

$$\eta(\tau)=\left[\frac{1}{(\tau^2/\alpha_1)+1}\right]\left[1-\frac{\beta_1\tau}{\tau^2+\alpha_2}+\frac{\beta_2\tau^2}{(\tau^2+\alpha_3)^2}\right], \tag{11}$$

TABLE I. Numerical values for the coefficients appearing in Eq. (11).

α_1	0.505
α_2	0.185
α_3	9.95
β_1	0.331
β_2	5.85

in which the five geometry dependent parameters ($\alpha_{1,2,3}$ and $\beta_{1,2}$) are chosen to give a good match to the exact numerical $\eta(\tau)$ function. The parameters we used in expression (11) are given in Table I for an infinite slab geometry. With these parameters, expression (11) agrees with the exact numerical $\eta(\tau)$ function to better than 5% at all optical depths $\tau(\omega)$. Note that this is a slightly different (and more accurate) fit than we used in Ref. 15. Under our conditions, escape factors can now be calculated rapidly for either of the line shapes mentioned. For an impact-broadened Lorentzian line shape without structure, the integral in Eq. (8) can be evaluated in closed form using Eq. (11):

$$g=\{[0.967\cos(\theta_1/2)+0.735\sin(\theta_1/2)]/\sqrt{R_1}\}-\{[1.214\sin(\theta_2/2)]/\sqrt{R_2}\}$$
$$+[([0.0331\cos(\theta_3/2)]-\{0.00249[\tau(\omega_0)/R_3]\sin(3\theta_3/2)\})/\sqrt{R_3}]\ . \tag{12}$$

Each of the parameters in the above equation depends simply on the line-center optical depth $\tau(\omega_0)$. These are given by

$$R_i=(\{[\tau(\omega_0)]^2/\alpha_i\}+1)^{1/2} \tag{13a}$$

and

$$\tan(\theta_i)=\tau(\omega_0)/\sqrt{\alpha_i}\ . \tag{13b}$$

The numerical coefficients in Eq. (12) are simple fractions involving the α_i and β_i of Eq. (11). The full closed-form expression for the Post-theory Lorentzian line-shape escape factor is given in the Appendix. This expression may be of use to those who wish to extend these results to different geometries. [i.e., Eq. (10) could be fit with a function of the form of (11) but with different numerical values for the parameters. The escape factor can then be obtained from Eq. (A1).] While Eq. (12) for g is complicated, it is more convenient in most cases than carrying out the numerical integration. Note that these Post-theory results for the impact-broadened Lorentzian, depend only on the line-center optical depth $\tau(\omega_0)$, and should be valid for all values of $\tau(\omega_0)$.

If we examine Eq. (12) in the high-optical-depth limit, we obtain

$$g=\frac{1.21}{[2\pi\tau(\omega_0)]^{1/2}}\ . \tag{14}$$

This equation should agree with the Holstein theory result Eq. (2b). In fact the two expressions differ only in the numerical constant (1.21 for Post versus 1.15 for Holstein). The difference in these constants is due to the different approximations used to derive these expressions.

For the Doppler-broadened Gaussian line shape, we were unable to obtain a closed-form expression from Eq. (8) for the escape factor, which would be valid over the entire range of optical depths. It may be possible to obtain a closed-form expression for the integral in Eq. (8) in the high-optical-depth limit. However we did not attempt to do this in the present work since our main concern was the low-optical-depth range.

III. THE EXPERIMENT

The experimental setup is shown in Fig. 1(a). Sodium vapor is contained in an oven formed from a stainless steel block drilled out to make a cross. Sapphire windows are sealed to the cell using silver O rings. Two arms of the cell are filled by sapphire rods whose end faces create a slab geometry for the vapor in the observation region [see Fig. 1(b)]. [The rod and window on each side are actually made from a single piece of sapphire.] The spacing between the two rod end faces, 0.55 cm, is small compared to their diameters of 1.27 cm. The cell body is uniformly heated (including the windows) to a fixed temperature of 675±5 K in order to avoid density gradients. The sodium vapor pressure is controlled by the temperature of a side arm, which is kept at a lower

temperature than the cell in order to prevent sodium from condensing on the windows. Inert gas can be added or removed from the cell through the attached vacuum and gas handling system. This allows us to alter the line shape in a controlled fashion.

The vapor is excited by a dye laser which produces pulses of ~0.4-Å bandwidth near 5890 Å. The dye laser, which is pumped by a nitrogen laser, has a pulse duration of ~0.5 ns and produces an output of ~130 μJ/pulse. Stainless steel aperatures inside the cell create an excitation geometry in which the laser beam nearly fills the entire observation region, but eliminates scatter of laser light from the sapphire rod end faces [see Fig. 1(b)]. Fluorescence is collected through a lens system and is dispersed with a 0.5 m monochromator [Fig. 1(c)]. The light is detected using a photomultiplier tube with an S-20 spectral response. The photomultiplier tube (PMT) output is recorded on a transient digitizer which is triggered by a photodiode [Fig. 1(a)]. The transient digitizer records and stores an entire fluorescence time decay with 512-point resolution. These data are then sent to a computer, where 256 traces are averaged. The time resolution of the complete system has been measured to be about 1.5 ns. A white light on the far side of the cell is used to measure absorption equivalent widths from which sodium densities are determined.

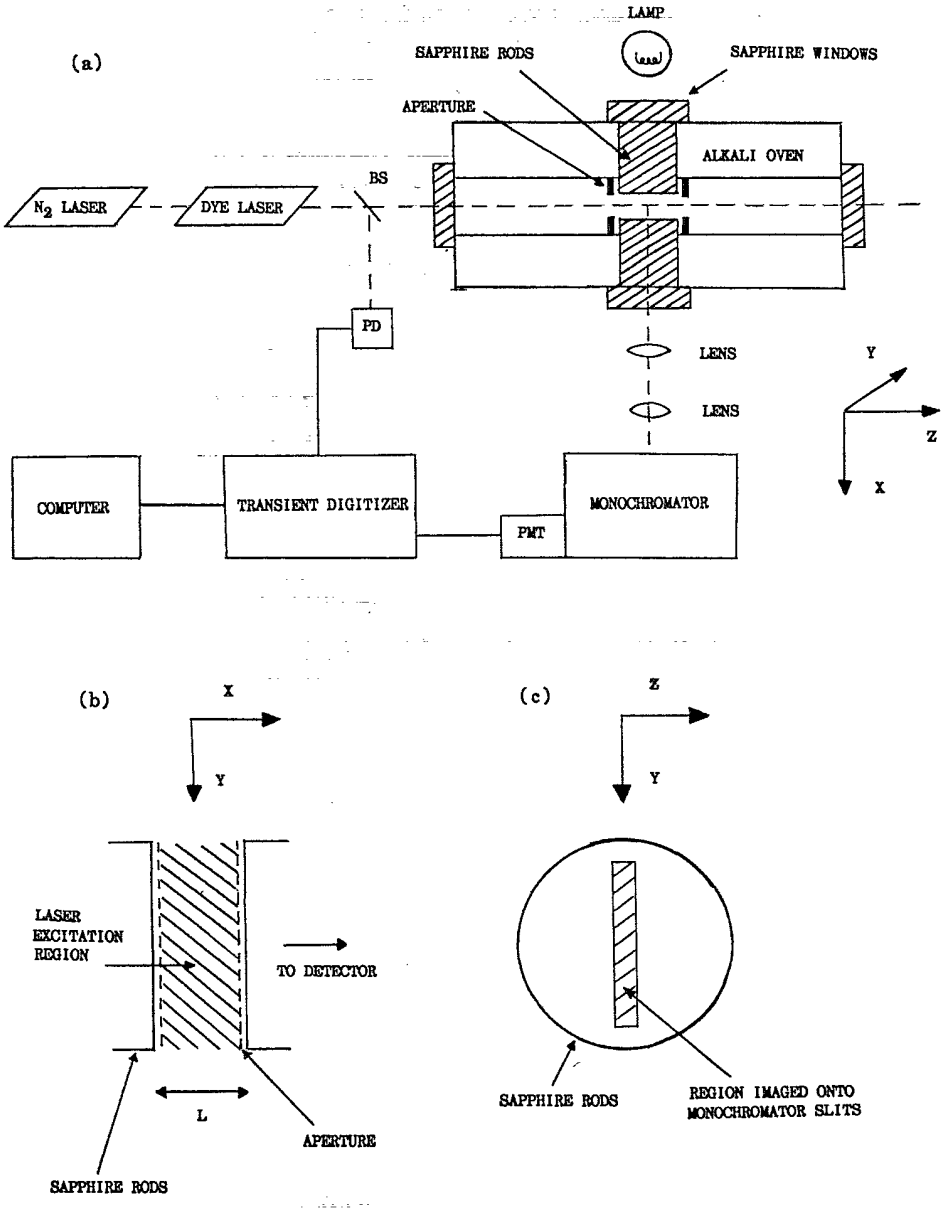

FIG. 1. (a) Experimental setup. BS, PD, and PMT indicate beam splitter, photodiode, and photomultiplier, respectively. (b) Cross section of the cell interior as viewed along the laser axis. The cross-hatched region represents the region excited by the laser. (c) Cross section of cell as viewed from the detector. The cross-hatched region indicates the region imaged onto the monochromator slits.

A data run in the foreign-gas Lorentzian line-shape experiment consists of at least two equivalent width measurements separated in time by one or more fluorescence decay rate measurements. These are done sequentially, with a fixed amount of argon gas sealed in the cell. A single run takes approximately thirty minutes. The before and after equivalent width measurements, with gas in the cell, are needed to insure that the sodium density has remained constant. Densities obtained from these equivalent width measurements (see Sec. IV A) typically agree to better than 10%. Their average is used in the analysis. Occasionally, equivalent widths are also recorded, as a check, before letting gas into the cell; i.e., in a pure sodium environment. Densities obtained from this method are consistent with the sodium-argon results, but tend to be less accurate.

In the Doppler line-shape experiment, the sodium density is also determined using equivalent widths. However, since the equivalent width may not be very sensitive to the density when the line is Doppler broadened, we use a slightly different procedure in this case. An equivalent width without foreign gas is taken, followed by the fluorescence time decay. This is followed by another equivalent width measurement taken with ~ 100 Torr of foreign gas present. The addition of this moderate amount of foreign gas does not perturb the sodium density significantly. In either experiment, these methods yield absolute sodium densities which are accurate to $\sim 10\%$.

Neutral density filters are occasionally inserted into the fluorescence channel to test for detector linearity, and into the laser beam to verify that nonlinear processes (for example, quenching by electrons created in associative ionization or photoionization) do not modify the decay rates. Laser and monochromator bandwidths are such that the D_1 ($3\,^2P_{1/2}\rightarrow 3\,^2S_{1/2}$) and D_2 ($3\,^2P_{3/2}\rightarrow 3\,^2S_{1/2}$) lines can easily be resolved.

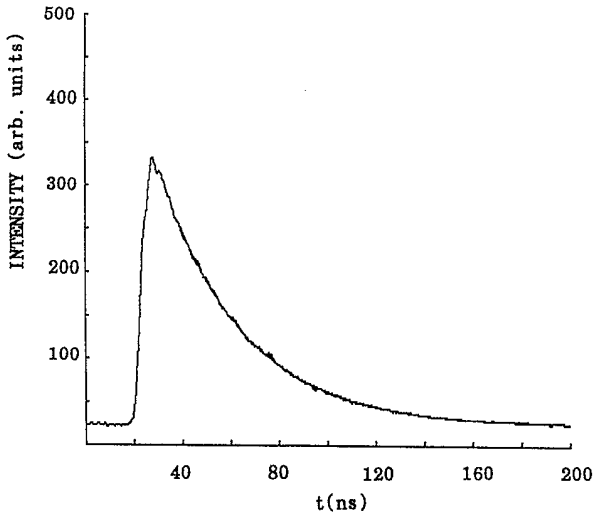

FIG. 2. Sodium D_2 line fluorescence intensity as a function of time (average of 256 laser pulses) along with a fitted exponential decay. The laser fired at $t\sim 20$ ns, and the fitted decay starts at $t_0\sim 40$ ns. The laser was tuned to the D_2 line, the sodium density was $\sim 1.86\times 10^{12}$ cm^{-3}, and the argon pressures was 259 Torr.

IV. RESULTS

A. General considerations

A typical fluorescence decay is shown in Fig. 2. In general, even when the radiative decay of each state can be described by single rate, the measured fluorescence decay rate ω_- will be a mixture of effective decay rates ($\Gamma_{1\text{eff}}$ and $\Gamma_{2\text{eff}}$) from the two sodium fine-structure levels which are collisionally mixed:

$$\omega_-=\xi\Gamma_{1\text{eff}}+(1-\xi)\Gamma_{2\text{eff}} . \tag{15}$$

The parameter ξ is determined by the statistical weights, collisional excitation transfer rates, and to a lesser degree by the collisional broadening rates. If we denote $3\,^2P_{3/2}$ as state 2 and $3\,^2P_{1/2}$ as state 1, then the populations of the two states can be described by the following rate equations which are valid once the laser pulse has terminated [for weak fields and for broadband excitation; i.e., we assume the ground-state density remains approximately constant, and that the laser pumps all velocity groups]:

$$\dot{n}_2=R_{12}n_1-(\Gamma_{2\text{eff}}+R_{21})n_2 , \tag{16a}$$

$$\dot{n}_1=R_{21}n_2-(\Gamma_{1\text{eff}}+R_{12})n_1 . \tag{16b}$$

Here the Γ_{eff}'s are the effective radiative rates given by Eq. (1), and the R's are the collisional excitation transfer rates which have a contribution from ground-state sodium atoms[17] and one from inert-gas perturbers:[18,19]

$$R_{21}=k_{21}^{\text{Na}}n+k_{21}^{p}n_p . \tag{17}$$

Equations (16) yield a double-exponential time dependence for the two upper states.[3,4] However, in the late time, both states decay as a single exponential with the slower of the two rates ω_-:[3,4]

$$\omega_-=\tfrac{1}{2}(\Gamma_{1\text{eff}}+\Gamma_{2\text{eff}}+R_{12}+R_{21}) -\tfrac{1}{2}[(\Gamma_{1\text{eff}}-\Gamma_{2\text{eff}})^2+2(R_{12}-R_{21})(\Gamma_{1\text{eff}}-\Gamma_{2\text{eff}}) +(R_{21}+R_{12})^2]^{1/2} . \tag{18}$$

In the limit of low collisional transfer, ω_- reduces to $\Gamma_{2\text{eff}}$ (i.e., $\xi=0$). On the other hand, in the complete mixing limit ($R\gg\Gamma_{\text{eff}}$), we find

$$\xi=[1+(g_2/g_1)\exp(-\Delta E/kT)]^{-1} ,$$

where $\Delta E=17$ cm^{-1} is the $3\,^2P_{1/2}$-$3\,^2P_{3/2}$ fine-structure splitting, and the principle of detailed balance has been used to fix the ratio of the two collisional transfer rates. For our cell temperature of 675 K, Eqs. (15) and (18) yield $\omega_-=0.341\Gamma_{1\text{eff}}+0.659\Gamma_{2\text{eff}}$ in the complete mixing limit.

Since the theoretical radiative rates $\Gamma_{1\text{eff}}$ and $\Gamma_{2\text{eff}}$ are fundamental mode decay rates, we must consider wheth-

er this is what we measure. In general, the laser excites some linear combination of spatial modes, which then decays as a sum of exponentials. Since the fundamental mode has the slowest decay rate, a pure fundamental mode can be achieved by simply waiting until the late time.[4] The time required to reach this condition is determined by the excitation geometry. In particular, the time is reduced by making a reasonable match between the laser transverse spatial profile and the fundamental mode spatial distribution. This increases the amplitude of the fundamental mode [C_1 in Eq. (4)] relative to that of the higher modes. Such a match is obtained in the present experiment by filling the slab region with laser light [see Fig. 1(b)]. For a typical scan, we fit a single exponential to the data beginning at some initial time t_0 (Fig. 2). We then repeat the fit using larger values of t_0 and continue until we find the decay rate converge to a constant value, which is the decay rate ω_- [Eq. (15) or (18)] for the fundamental mode.

We tested the effects of a poor match to the fundamental mode by focusing the laser to a tight excitation beam. The position of the focus was varied across the slab region. Even with this very poor match to the fundamental mode, the fitted late-time decay rates differ by less than 20% for different focus positions and compared to the filled-slab excitation. The latter was used to produce all results reported here.

Sodium atom densities must be known in order to compare theoretical and experimental decay rates. As stated in Sec. III, these are determined using absorption equivalent width measurements.[11,20] Measured values are compared to equivalent widths calculated using a Voigt line shape and including hyperfine structure. Calculated values for the sodium D_2 line ($3\,^2S_{1/2}\rightarrow 3\,^2P_{3/2}$) equivalent width versus sodium density are shown for a path length $L=0.55$ cm and $T=675$ K in Fig. 3. The lower solid curve corresponds to the case of pure sodium. The upper solid curve corresponds to the case where the line always remains optically thin; that is, the line is extremely broadened (infinite foreign-gas pressure limit). In this case, the equivalent width is determined simply by the normalization condition $\int k(\omega)d\omega=\kappa$ [see Eq. (3)]. The intermediate dashed curves represent different values of the foreign-gas broadening rate. Thus each dashed curve corresponds to a different foreign-gas pressure, which can be identified if the particular pressure-broadening coefficient is known. The self-broadening rate for the sodium D_2 line is also necessary for the calculations, and is taken from Ref. 21. For a given inert gas pressure (for which the sodium D_2 line-broadening rates are known[22]) we are able to read accurate sodium densities off Fig. 3 directly. Note that the foreign-gas broadening rates must be scaled to our cell temperature of 675 K, which is done using the theoretical $T^{0.3}$ temperature dependence.[23] The self-broadening rates are expected to be independent of temperature.[24]

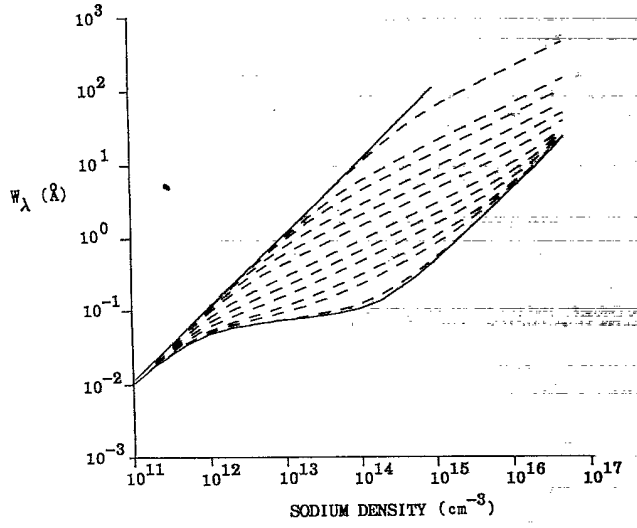

FIG. 3. Sodium D_2 line equivalent widths vs sodium density. Calculations were carried out for a Voigt line shape, with an absorption length of 0.55 cm and a cell temperature of 675 K. The upper solid curve represents the optically thin limit (infinite foreign-gas pressure limit), while the lower solid curve corresponds to the pure sodium case. The intermediate dashed curves correspond to different foreign-gas broadening rates. From the top down these are 1×10^{13}, 1×10^{12}, 5×10^{11}, 2×10^{11}, 1×10^{11}, 5×10^{10}, 2×10^{10} 1×10^{10}, 5×10^{9}, 2×10^{9}, 1×10^{9}, and 1×10^{8} s^{-1}. [Note these values represent the foreign-gas broadening contributions to the Lorentzian full width at half maximum only.]

B. Lorentzian line shape [$k(\omega_0)L/2\lesssim 10$]

At high foreign-gas densities, the $3\,^2P_{1/2}$ and $3\,^2P_{3/2}$ populations are completely mixed by collisions, and the entire line shape for each fine-structure component can be described as a pressure-broadened Lorentzian. In order for this approximation to be valid, the argon pressure must be low enough that satellites and other non-Lorentzian features remain far outside the unity optical depth points. In addition, the pressure-broadened linewidth must be much larger than either the Doppler linewidth or hyperfine structure splittings; i.e., $\Gamma_c \gg \Delta\omega_D$, $\Delta\omega_{hfs}$. (The ground-state hyperfine splitting of 1.772 Ghz is much larger than those of the excited states and is roughly equal to the Doppler width.) For sodium densities between 5×10^{11} and 5×10^{13} cm^{-3} and argon pressures of 500 to 7000 Torr, as used in this experiment, the line shape is well approximated by an impact-broadened Lorentzian function, which is valid over the entire part of the line relevant to the radiation trapping process [i.e., $0.1<k(\omega)L/2<5$]. For these experimental conditions, the simple foreign-gas-broadened Lorentzian line shape (neglecting self, natural, and Doppler broadening, as well as hyperfine structure) and the full Voigt line shape (including all these effects) agree to within 8% in the relevant part of line, for the worst case (i.e., the lowest argon densities). Even then, disagreement only occurs for a small region near line center. As the argon pressure increases, the approximation becomes even better. Such extreme pressure broadening has the effect of dramatically reducing the line-center optical depth. For example, when the sodium

density is 5×10^{13} cm^{-3}, the line-center optical depth $k(\omega_0)L/2$ is reduced from ~115 to ~2 by the addition of 7000 Torr of argon.

Due to the rapid mixing between the two fine structure levels (the excitation transfer rates are at least 4×10^9 s^{-1} for 500 Torr of argon, while the fastest radiative decay is limited by the natural radiative rate[25] 6.3×10^7 s^{-1}), ω_- should be independent of which transition is pumped and which is observed. Most of the data presented here were taken for excitation of the sodium $3\,^2S_{1/2}-3\,^2P_{3/2}$ transition and observation of the same transition in fluorescence. However, data were taken periodically in which the $3\,^2S_{1/2}-3\,^2P_{1/2}$ transition was either pumped or detected in order to verify the above statements. Due to this high rate of collisional mixing, the observed decay rates should be accurately described by Eq. (15) with $\xi=0.341$.

The experimental results are shown in Fig. 4. The measured decay rates ω_- are plotted against the line-center optical depth $k(\omega_0)L/2$ which is calculated from Eqs. (3) and (9b) for a Lorentzian line shape [i.e., $k(\omega_0)L/2=\kappa L/(\pi\Gamma_c)$]. Also plotted are decay rates calculated using Eq. (15) and the Post, Milne, and Holstein theories. We note that the Milne theory agrees well with the more accurate Post theory for low optical depths when Milne's geometric factor l is chosen to be equal to the slab thickness L as in Eq. (6). The Milne theory agrees well with our experimental results for optical depths up to about 5. On the other hand, the Post theory shows good agreement with the experiment over the entire range of optical depths tested here. We note that the Holstein theory expression breaks down and gives nonphysical results when the optical depth is reduced below ~0.3. For $k(\omega_0)L/2\gtrsim1$, the Holstein and Post theories

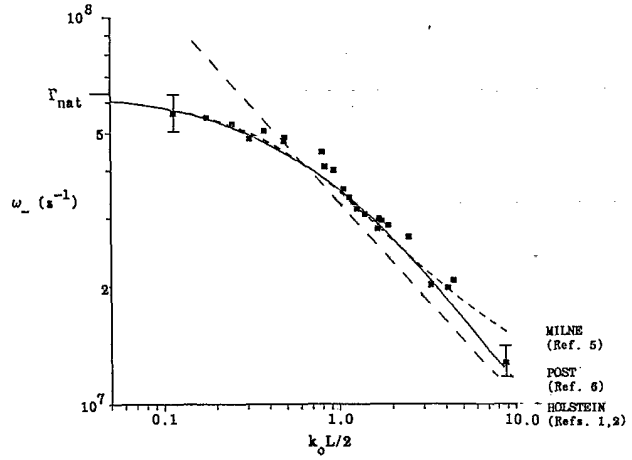

FIG. 4. Measured sodium D_2 line late-time fluorescence decay rates ω_- plotted against the Lorentzian line-center optical depth $k(\omega_0)L/2$. The sodium density and argon pressures were varied over the ranges of $5\times10^{11}<n<5\times10^{13}$ cm^{-3} and $500<P_{Ar}<7000$ Torr, respectively. The cell temperature was fixed at 675±5 K. Also shown are predictions of ω_- obtained from the Holstein (long-dashed line), Milne (short-dashed line), and Post (solid line) theories. Error bars are shown for a couple of points.

agree reasonably well with each other. As stated earlier, these are expected to agree for higher optical depths [see Eqs. (2b) and (14)]. The Holstein theory has been tested previously in the much higher range of optical depths $2<k(\omega_0)L/2<1000$, where it also agreed well with experiment.[3,4]

C. Doppler line shape [$k(\omega_0)L/2\lesssim10$]

For a pure sodium environment at low densities, the line shape is well described by the Doppler Gaussian. As above, most measurements of the fluorescence decay rates are made when pumping and observing the $3\,^2S_{1/2}-3\,^2P_{3/2}$ transition. The Doppler linewidth is determined by the temperature of the cell, and changes in the Doppler width due to temperature fluctuations are negligible. Under our conditions of no foreign gas and sodium densities less than 5×10^{12} cm^{-3}, we find that the pure Doppler line shape (including only the hyperfine structure) agrees with the full Voigt function (including natural and self-broadening as well as the hyperfine structure) to within 5% in the worst case for the part of the line most critical to the trapping process ($0.1<k(\omega)L/2<5$). The natural and self-broadened Lorentzian contributions to the linewidth are very small compared to the Doppler contribution under these conditions, except in the far wings where negligible trapping occurs. The effects of hyperfine structure must, however, be included under these conditions, since the splitting of the hyperfine components is nearly equal to the Doppler width.

Fluorescence decay rates were measured for sodium densities in the range of 5×10^{10} to 5×10^{12} cm^{-3} without foreign gas present. Here the collisional excitation transfer rates for these sodium densities and in the absence of any foreign gas ($\sim1\times10^4$ s^{-1} for the highest sodium density[17]) are small compared to the effective radiative rates ($\Gamma_{eff}\gtrsim4\times10^6$ s^{-1}). In fact, under these conditions, the D_1 fluorescence intensity is less than 1% of that observed for the D_2 line. Thus the observed experimental decay rate ω_- is actually just Γ_{2eff} rather than the weighted average of Γ_{1eff} and Γ_{2eff} obtained in the complete mixing limit [i.e., $\xi=0$ in Eq. (15)].

Figure 5 shows a comparison between decay rates measured in the no foreign-gas, low sodium density limit, and those calculated from theory. Here the decay rates are again plotted against sodium D_2 line-center optical depth $k(\omega_0)L/2$ which is calculated from Eq. (3) and the Doppler line-shape function, Eq. (9a), but neglecting hyperfine structure; {i.e., $k(\omega_0)L/2=\kappa L[\ln(2)/\pi]^{1/2}/\Delta\omega_D$}. The hyperfine structure is, however, taken into account in the theoretical treatments of the decay rates. (This occurs naturally in the Milne and Post theories by simply including the hyperfine structure into the line-shape function $F(\omega)$ in Eqs. (5) and (8). In the Holstein theory, we have included hyperfine structure in an *ad hoc* manner by simply replacing $k(\omega_0)$ (calculated without considering hyperfine structure as above) in Eq. (2a) by $k_{max}(\omega)$, which is the true maximum absorption coefficient when hyperfine structure is included [note: $k_{max}(\omega)\sim\frac{5}{8}k(\omega_0)$ under these conditions.[3,15]]) As in the

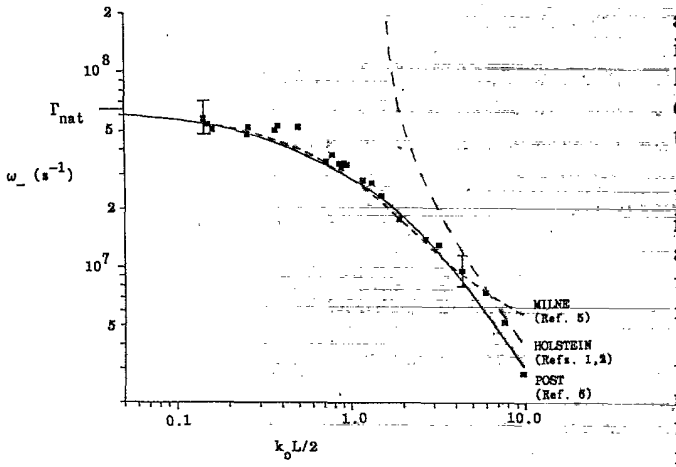

FIG. 5. Measured sodium D_2 line late-time fluorescence decay rates ω_- plotted agsint the Doppler line-center optical depth $k(\omega_0)L/2$. In this case, no foreign gas was present, and changes in the optical depth were made by varying the sodium density over the range $5\times10^{10}<n<5\times10^{12}$ cm^{-3}. The cell temperature was fixed at 675±5 K. [The line-center optical depth $k(\omega_0)L/2$ plotted on the horizontal axis is for a Doppler line without hyperfine structure.] Also shown are the predictions of ω_- using the Holstein (long-dashed line), Milne (short-dashed line), and Post (solid line) theories. Details of the line shape, including hyperfine structure, are taken into account in the theories as described in the text. Error bars are shown for a couple of points.

case of the pure Lorentzian line shape, the Post theory agrees well with experiment over the whole range of optical depths studied, while the Milne theory agrees only at low optical depths [$k(\omega_0)L/2\lesssim8$]. The Holstein theory is seen to be unreliable for optical depths below ~3. The disagreement between the Post and Holstein theories at higher optical depths is due to the *ad hoc* manner in which we have accounted for the hyperfine structure in the Holstein theory.[15]

D. Uncertainties

In Figs. 4 and 5 error bars are placed on a couple of the data points. We must consider several possible sources of error in order to determine the accuracy of our measurements.

The sodium densities obtained using the techniques described above should be accurate to ~10%. The uncertainty in the argon pressure is less than 1%. Our results are not sensitive to the excitation transfer rates since the two regimes we studied involve either complete mixing or no mixing of the fine-structure level populations.

The time response of the detection system was measured to be ~1.5 ns, which introduces a 10% uncertainty in measured ω_- values for the fastest decays. The presence of higher spatial modes in the sense of Eq. (4) may also have some effect on the measured decay rates, although the magnitude of this effect is reduced by the pump beam geometry. We estimate the effect to be less than 5% for our conditions. Window reflectivity may also affect the decay rates, since photons reflected back into the vapor make the cell effectively larger. From known reflectivity of sapphire and the theoretical dependence of the decay rates on L, we estimate the uncertainty in the decay rates at ~5–10 % from this effect.

Finally, the statistical uncertainty of the data and of the fitting routine are estimated at less than 5%. Assuming that these sources of uncertainty are uncorrelated, and considering the dependence of the decay rates on these parameters, we estimate that the experimentally measured decay rates are accurate to ~15%.

In addition to the above considerations, we should note that quenching collisions provide an alternate decay mechanism for excited atoms, which competes with spontaneous emission. However, these quenching mechanisms are not included in the overall decay rate uncertainties listed above. The following arguments show that quenching mechanisms have a negligible effect on the trapped decay rates for our experimental conditions.

Quenching may occur when energy from an excited sodium atom is collisionally transferred to either a sodium dimer, an argon atom, or an impurity atom or molecule which is present in the cell. For these experiments, the Na_2 density is less than 3×10^{11} cm^{-3}.[26] Thus, the $Na_2+Na^*\rightarrow Na_2^*+Na$ quenching rate is less than 10^3 s^{-1} (assuming a rate coefficient of 3.4×10^{-9} cm^{3}s^{-1} from Ref. 27) which will affect our observed decay rates negligibly.

The cross section for quenching of sodium by noble gases has been shown to be less than 10^{-18} cm^2 by Copley, Kibble, and Krause.[28] Using this as an upper limit, we find that quenching by argon could affect our measured decay rates in the worst case by 20%. We note that such quenching by argon would, however, cause a linear dependence of the decay rates on argon pressure, and could actually give decay rates which are faster than the natural radiative rate at high pressures. Since neither of these effects was observed, our results suggest that the cross section for quenching of sodium by argon is actually smaller than the value used above.

Impurities in the argon, especially diatomic molecules, can be very efficient quenchers. For example, experimental values in the range 1×10^{-15} to 5×10^{-15} cm^2 (Refs. 29–33) have been reported for the cross section for quenching of Na(3P) by N_2. The purity of the argon used in the present experiments is 99.999%. If we assume that all impurities quench with the cross section of 5×10^{-15} cm^2, then the worst case effect on decay rates is only 3%. Again, if this type of quenching dominates the decay rates, we expect a linear dependence of decay rates on argon pressure, and possibly decay rates which exceed the natural radiative rate. As discussed above, neither of these effects was observed.

Impurities present in the vacuum system and cell may also lead to quenching of Na(3P). Here, these impurities would be expected to build up with time after the cell is sealed off from the vacuum pumps. Thus we might expect to observe an increase in measured decay rates with time following the sealing of the cell. However, no noticeable change in the decay rates was seen after the cell had been sealed for over 90 minutes, which is longer than

the typical time the cell remained sealed during data runs. Thus we conclude that these quenching mechanisms also do not affect our results.

V. CONCLUSIONS

We have measured effective decay rates of resonance radiation under conditions of low to moderate line-center optical depth. The conditions were such that the line shape could be described by a single line-broadening mechanism: either Doppler, or impact-regime pressure broadening. In both cases, the approximation of complete frequency redistribution is valid. For these simple line shapes, calculations of effective radiative rates using any of the theories discussed, are greatly simplified. The measured decay rates demonstrate the range of optical depths over which each of the theories is valid.

For the impact-broadened Lorentzian line shape, the Post theory gives good agreement with experiment over the entire range of optical depths. An approximate expression for Post theory decay rates under these conditions (and assuming complete frequency redistribution) is given in this paper. The Milne theory is shown to work well only at low optical depths, and agrees with the Post theory in that range. At high optical depths, we have previously verified that the Holstein theory works well, agreeing with the Post theory in that range.

For the Doppler-broadened Gaussian line shape, the Post theory results also agree with measured decay rates over the range of low to moderate optical depth. In the low optical depth region, the Milne and Post theories again give similar results. In our use of both of these theories, hyperfine structure is explicitly taken into account, and complete frequency redistribution is assumed. At higher optical depths, data from our previous work agrees best with Holstein theory expressions in which hyperfine structure was taken into account in an *ad hoc* manner.

Finally, by looking at Figs. 4 and 5, one can see that the escape factor is quite different for equal line-center absorption coefficients, but different line shapes. Thus, knowledge of the line-center absorption coefficient by itself is not sufficient to predict the effective radiative rate.

ACKNOWLEDGMENTS

The authors would like to thank Dr. Alan Streater for many helpful discussions. We would also like to acknowledge financial support for this work from General Electric Corporate Research and Development, GTE Laboratories, and the National Science Foundation under Grant No. PHY-8451279.

APPENDIX

The full closed-form Post theory escape factor for a pure Lorentzian lineshape [Eq. (12)] is given here in terms of the α_i,β_i parameters of Eq. (11) and Table I, and the R_i and θ_i parameters of Eqs. (13):

$$g=\left\{\left[\left[1-\frac{\beta_2\alpha_1^{-1}}{[(\alpha_3/\alpha_1)-1]^2}\right]\cos(\theta_1/2)+\left[\frac{\beta_1\alpha_1^{-1/2}}{1-(\alpha_2/\alpha_1)}\right]\sin(\theta_1/2)\right]R_1^{-1/2}\right\}-\left\{\left[\left[\frac{\beta_1\alpha_2^{-1/2}}{1-(\alpha_2/\alpha_1)}\right]\sin(\theta_2/2)\right]R_2^{-1/2}\right\}$$
$$+\left\{\left\{\left[\left[\frac{\beta_2\alpha_1^{-1}}{[(\alpha_3/\alpha_1)-1]^2}\right]\cos(\theta_3/2)\right]-\left[\left[\frac{\beta_2\alpha_3^{-3/2}}{4[(\alpha_3/\alpha_1)-1]}\right][\tau(\omega_0)/R_3]\sin(3\theta_3/2)\right]\right\}R_3^{-1/2}\right\}. \quad \text{(A1)}$$

[1]T. Holstein, Phys. Rev. **72**, 1212 (1947).
[2]T. Holstein, Phys. Rev. **83**, 1159 (1951).
[3]J. Huennekens and A. Gallagher, Phys. Rev. A **28**, 238 (1983).
[4]J. Huennekens, H. J. Park, T. Colbert, and S. C. McClain, Phys. Rev. A **35**, 2892 (1987).
[5]E. A. Milne, J. London Math. Soc. **1**, 40 (1926).
[6]H. A. Post, Phys. Rev. A **33**, 2003 (1986).
[7]J. B. Anderson, J. Maya, M. W. Grossman, R. Lagushenko, and J. F. Waymouth, Phys. Rev. A **31**, 2968 (1985).
[8]C. van Trigt, Phys. Rev. **181**, 97 (1969).
[9]C. van Trigt, Phys. Rev. A **13**, 726 (1976).
[10]H. A. Post, P. van de Weijer, and R. M. M. Cremers, Phys. Rev. A **33**, 2017 (1986).
[11]A. C. G. Mitchell and M. W. Zemansky, *Resonance Radiation and Excited Atoms* (Cambridge Press, Cambridge, 1971).
[12]B. P. Kibble, G. Copley, and L. Krause, Phys. Rev. **153**, 9 (1967).
[13]R. P. Blickensderfer, W. H. Breckenridge, and J. Simons, J. Phys. Chem. **80**, 653 (1976).
[14]M. G. Payne, J. E. Talmage, G. S. Hurst, and E. B. Wagner, Phys. Rev. A **9**, 1050 (1974).
[15]J. Huennekens and T. Colbert, J. Quant. Spectrosc. Radiat. Transfer, **41**, 439 (1989).
[16]A. Streater, J. Cooper, and W. Sandle, J. Quant. Spectrosc. Radiat. Transfer, **37**, 151 (1987).
[17]J. Huennnekens and A. Gallagher, Phys. Rev. A **27**, 1851 (1983).
[18]R. Seiwert, Ann. Phys. (Leipzig) **18**, 54 (1956).
[19]J. Pitre and L. Krause, Can. J. Phys. **45**, 2671 (1967).
[20]A. Corney, *Atomic and Laser Spectroscopy* (Clarendon, Oxford, 1977).
[21]C. G. Carrington, D. N. Stacey, and J. Cooper, J. Phys. B **6**, 417 (1973).
[22]J. F. Kielkopf, J. Phys. B **13**, 3813 (1980).
[23]N. Lwin, D. G. McCartan, and E. L. Lewis, Astrophys. J. **213**, 599 (1977).
[24]H. G. Kuhn, *Atomic Spectra* (Academic, New York, 1969).
[25]W. L. Wiese, M. W. Smith and B. M. Miles, *Atomic Transition Probabilities*, Nat. Bur. Stand. Ref. Data. Ser., Natl. Bur. Stand. (U.S.) Circ. No. 22 (U.S. GPO, Washington, D.C.,

1969), Vol. II.
[26]A. N. Nesmeyanov, *Vapor Pressure of the Elements* (Academic, New York, 1963).
[27]L. K. Lam, T. Fujimoto, A. C. Gallagher, and M. M. Hessel, J. Chem. Phys. **68**, 3553 (1978).
[28]G. Copley, B. P. Kibble, and L. Krause, Phys. Rev. **163**, 34 (1967).
[29]S. Tsuchiya and K. Kuratani, Combust. Flame **8**, 299 (1964).
[30]W. Demtroder, Z. Phys. **166**, 42 (1962).
[31]B. P. Kibble, G. Copley, and L. Krause, Phys. Rev. **159**, 11 (1967).
[32]R. G. W. Norrish and W. M. Smith, Proc. R. Soc. London, Ser. A **176**, 295 (1941).
[33]I. Tanarro, F. Arqueros, and J. Campos, J. Chem. Phys. **77**, 1826 (1982).